J Nanostruct Chem (2015) 5:313–323
DOI 10.1007/s40097-015-0163-0

ORIGINAL RESEARCH

Fe doping effects on the structural, magnetic, and magnetocaloric properties of nano-sized $Pr_{0.6}Bi_{0.4}Mn_{1-x}Fe_xO_3$ ($0.1 \leq x \leq 0.3$) manganites

K. Sbissi[1] · V. Collière[2] · M. L. Kahn[2] · E. K. Hlil[3] · M. Ellouze[4] · F. Elhalouani[1]

Received: 17 April 2015 / Accepted: 9 June 2015 / Published online: 22 June 2015

Abstract The structural, magnetic, and magentocaloric properties are systematically investigated for $Pr_{0.6}Bi_{0.4}Mn_{1-x}Fe_xO_3$ ($0.1 \leq x \leq 0.3$) manganites. The samples have been synthesized by sol–gel method. X-ray diffraction (XRD), scanning electron microscopy, transmission electron microscopy, and Fourier transform infrared spectroscopy were employed to investigate the crystalline structure. Magnetization measurements were used to investigate the magnetic properties. All the samples crystallize in the orthorhombic *Pnma* space group as expected for manganite compounds. The presence of a $PrMn_2O_5$ compound is also evidenced by XRD. The average size of the manganite particles is about 50–60 nm. Particle characterizations at the atomic level turn to be of paramount importance. Magnetic measurements versus temperature under an applied magnetic field of 0.01 T show that all samples exhibit a paramagnetic–ferromagnetic transition. Temperature-dependent magnetization measurements and Arrott analysis reveal second-first order ferromagnetic transitions for ($x = 0.1$ and $x = 0.2$). The magnetic entropy change $|\Delta S_M|$ was estimated using Maxwell relation method and is found to reach maximum values of 0.47 and 0.37 J/kg/K under an applied magnetic field of 5 T for $x = 0.1$ and $x = 0.2$, respectively.

Keywords Sol–gel synthesis · Manganites · Magnetization · Magnetocaloric effect

✉ K. Sbissi
sbissi2009@gmail.com

[1] National Engineering School of Sfax, University of Sfax, B. P. W-3038, Sfax, Tunisia

[2] Laboratory of Coordination Chemistry, 31077 Toulouse, France

[3] Institute Neel, CNRS and Joseph Fourier University, BP 166, 38042 Grenoble Cedex 9, France

[4] Faculty of Sciences, Sfax University, B. P. 1171, 3000 Sfax, Tunisia

Introduction

Since the discovery of the magnetocaloric effect (MCE) in the pure Gadolinium, numerous materials have been the subject of intensive study in order to improve their magnetocaloric properties and to propose them as potential candidate materials for magnetic refrigeration [1, 2]. Owing to their substantial MCE, the perovskite manganites with the general formula $Ln_{1-x}A_xMnO_3$, where Ln is a rare earth ion (Ln = La, Pr, Sm …) and A is a divalent element (A = Ca, Sr, Ba …), have attracted great interest for their colossal magnetoresistance (CMR) and MCE [3–6]. In fact, magnetic refrigeration is becoming a promising technology to replace the conventional gas compression–expansion technique. For sub-room temperature magnetic refrigeration applications, gadolinium is the first material known to show a large MCE, since it exhibits a maximum value of magnetic entropy change, ΔS_M^{max}, of 5 J/kg K at 294 K under an applied magnetic field of 2 T [1]. As it is well known, their essential magnetic properties are explained by the double exchange (DE) interaction between Mn^{3+} and Mn^{4+} ions and phase separation [7].

In addition, several perovskite manganites exhibit a transition from ferromagnetic to paramagnetic (PM) state near the Curie temperature where the MCE reaches a maximum. The correlation between both structure and magnetic properties is easily revealed and accorded by different elaboration methods.

Among these methods, the sol–gel method considered in this research work shows high ability to control the Curie temperature by substitution of ions in such manganites. In the present paper, we report the synthesis, structure, and magnetic properties of $Pr_{0.6}Bi_{0.4}Fe_xMn_{1-x}O_3$ nanostructured samples elaborated by sol–gel method.

Experimental section

Preparation of samples

The $Pr_{0.6}Bi_{0.4}Fe_xMn_{1-x}O_3$ ($0.1 \leq x \leq 0.3$) samples were prepared by a modified sol–gel method [8, 9]. Mixtures of Pr_6O_{11}, MnO_2, Bi_2O_3, and Fe_2O_3 with up to 99.9 % purity in stoichiometric proportions are used in the desired proportion according to the following reaction:

$$0.1\ Pr_6O_{11} + 0.2\ Bi_2O_2 + (1-x)\ MnO_2 + x/2\ Fe_2O_3 \rightarrow Pr_{0.6}Bi_{0.4}Mn_{1-x}Fe_xO_3 + \delta CO_2.$$

The precursors were dissolved in dilute 1 M HNO_3. Afterward, 3 g of citric acid and 1 mL of ethylene glycol were added and a complete homogenous transparent solution was achieved. Then, the solution was heated on thermal plate under constant stirring at 80 °C to eliminate the excess of water and to obtain a viscous gel [10]. Finally, the powders were grinded in an agate mortar and annealed at 900 °C for 4 h [11].

Characterization techniques

Fourier transformation infrared spectroscopy

To interpret the different vibrational modes, involving pairs/groups of atoms and the functional groups existing in the prepared $Pr_{0.6}Bi_{0.4}Fe_xMn_{1-x}O_3$ perovskite samples, Fourier Transformation Infra Red (FTIR) spectra were recorded using a spectrometer (Perkin Elmer 1725). The spectra were recorded in the wavenumber range of 4000–400 cm^{-1} at room temperature, in different reflectance modes, at a resolution of 1 cm^{-1}. The samples used for the measurements were obtained using the KBr pellet method. The KBr discs were made by pressing the mixture, which contained 10 mg of samples with 100 mg of KBr, at a pressure of 125 kg/cm^2.

Microscopy

The microstructure and morphology of the $Pr_{0.6}Bi_{0.4}Fe_xMn_{1-x}O_3$ samples were analyzed using SEM images obtained from scanning electron microscope (JEOL JSM 6700F). The spectrometer was operated at an accelerating voltage of 5 kV. A transmission electron microscope (TEM, JEOL JEM 2100F) was used to obtain substructural information and particle size of the prepared samples by recording TEM images and EDX. The samples for TEM studies were prepared ultrasonically by dispersing the samples in methanol.

X-ray diffraction

Phase purity, homogeneity, and crystal properties were determined by powder X-ray diffraction (XRD) at room temperature using a MPDPro Panalytical diffractometer equipped with CuKα (1.54056 Å) radiation. An additional powder XRD data for the powder calcined at 900 °C for 4 h was collected at ambient temperature in the range 10–70 in the 2θ domain with a 0.02 step and a 600 s per step counting time.

Magnetic measurements

Magnetization measurements versus temperature and magnetic field were recorded using a SQuID Magnetometer (MPMS 5 QUANTUM DESIGN (cryo-magnet 5T; cryostat 2–400 K). The evolution of the magnetization with temperature was recorded in the 2–300 K range, under an applied field of 10 Oe. The magnetization versus magnetic applied field measurements were recorded up to 5 T at several temperatures.

Results and discussions

Synthesis

During the synthesis, the sample is an uncolored sol, then the gel turns yellowish, and after precipitation, pulverulent dark brown powders are obtained. After sintering at 900 °C, any significant modification is observed: the samples are pulverulent dark brown powders. Yield ranges from 88, 89, to 92 %, respectively, for $x = 0.1$, $x = 0.2$ and $x = 0.3$, pointing out the efficiency of the sol–gel method.

FTIR spectroscopic investigations

Among numerous applications of vibrational spectroscopy to solid-state problems, those dealing with structural evolution of samples obtained by sol–gel process appear particularly interesting. IR spectroscopy gives qualitative information about the way in which the adsorbed molecules are bounded to the surface as well as structural

information of solids. Figure 1 shows FTIR spectra of the different $Pr_{0.6}Bi_{0.4}Fe_xMn_{1-x}O_3$ systems.

Figure 1a shows an example of the as-prepared sample for $x = 0.3$. The absorption bands in the 4000–1000 cm^{-1} range are characteristic of –OH, C=O, N–H, and CH_3 functional organic groups, while the region between 1000 and 400 cm^{-1} is the fingerprint of the inorganic material. The observed broad bands at 3400 and 2320 cm^{-1} can be attributed to the O–H stretching vibration of water molecules [12–14]. The bands at 1500 and 1066 cm^{-1} are ascribed to the stretching vibrations of the aliphatic CH_3 groups [15]. The bands between 900 and 400 cm^{-1} are mainly due to metal oxide bonds (Bi–O, Fe–O and Mn–O). Similar results are obtained for $x = 0.1$ and $x = 0.2$.

The FTIR spectra of the sintered samples displayed in Fig. 1b show only two bands. The 960 cm^{-1} band is assigned to the vibrations of COOH. The observed broad peak in the low wavenumber range of 560 cm^{-1} is characteristic of the Mn–O group [16] and can be attributed to the MnO_2 layers linked to the perovskite layers. When the sample was heat treated at 900 °C for 4 h, the absorption characteristic of νO–H stretching vanished, due to water evaporation from the surface of the powder. Our results are comparable to those obtained by Sana et al. [21] for $Pr_{0.6}La_{0.1}Ca_{0.3}Mn_{1-x}Fe_xO_3$ prepared by sol–gel method and Abir et al. [17] for $Pr_{0.6}Sr_{0.4}Mn_{1-x}Fe_xO_3$ prepared by ball Milling and evidence the formation of the desired manganites.

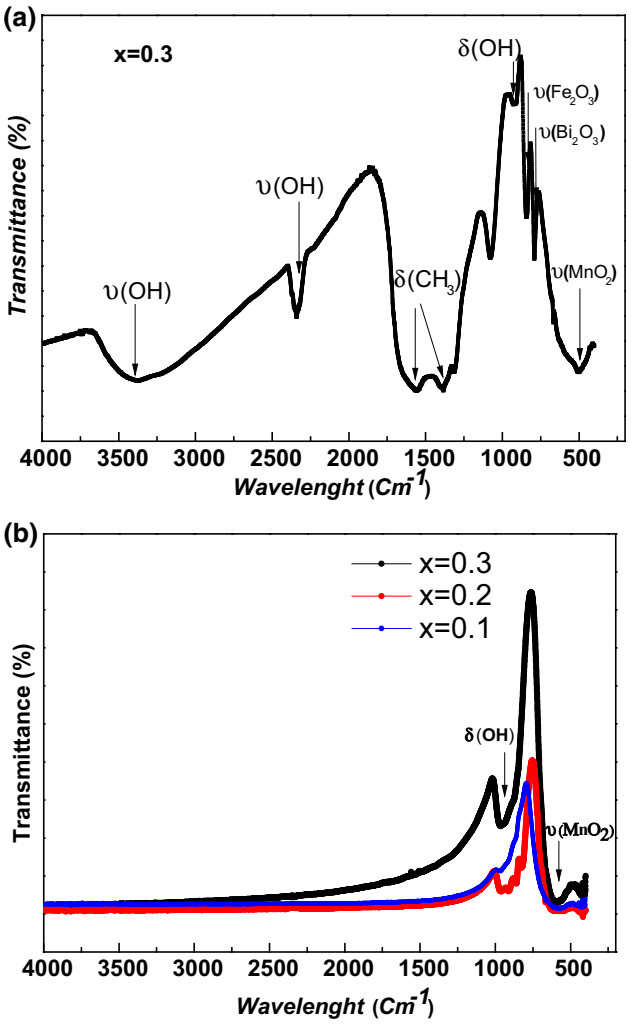

Fig. 1 FTIR vibration spectrum of $Pr_{0.6}Bi_{0.4}Fe_xMn_{1-x}O_3$ **a** as-made and **b** calcined powder

Structural properties

Phase identification and structural analysis were carried out by XRD technique with Cu Kα radiation at room temperature. The XRD patterns of $Pr_{0.6}Bi_{0.4}Fe_x$ $Mn_{1-x}O_3$ heated at 900 °C for 4 h (Fig. 2) show that all the samples crystallize in the orthorhombic structure with Pnma space group. The identification revealed the coexistence of two structures. The first one corresponding to $PrMn_2O_5$ fitted in the orthorhombic structure with the Pbam *space* group [18–20]. The second phase fits with Pbnm space group (JCPDS files 00-054 0871) and corresponds to the expected orthorhombic perovskite structure associated to the $Pr_{0.6}Bi_{0.4}Fe_xMn_{1-x}O_3$ [21]; the percentage of the secondary phase is nearly constant and is around 20 %. Precisely, the yield ranges from 22.5, 20.9 to 18.9 %, respectively, for $x = 0.1$, $x = 0.2$ and $x = 0.3$.

The average particle diameter, D, was obtained using Scherer's formula [22] for the peak width broadening as a function of the size of the particles.

$$D = \frac{K\lambda}{\beta\cos(\theta)}, \quad (1)$$

where λ (Cu $K\alpha = 1.5418$Å) is the X-ray wavelength, k is the machine constant (0.916), θ and β are the diffraction angle

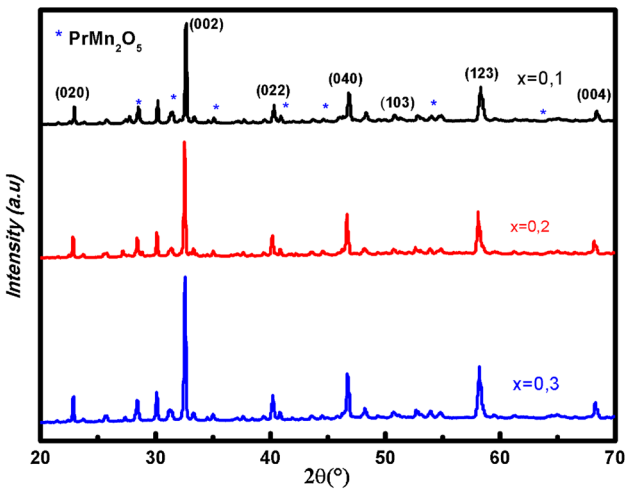

Fig. 2 X-ray diffraction patterns of $Pr_{0.6}Bi_{0.4}Fe_xMn_{1-x}O_3$ ($x = 0.1$, $x = 0.2$ and $x = 0.3$) compounds

and the full width for the most intense peak. The obtained D values are about 60 nm regardless of the compounds.

Transmission electron microscopy

In order to better evidence the particle size of $Pr_{0.6}Bi_{0.4}Fe_xMn_{1-x}O_3$ powders obtained by the sol–gel method, transmission electron microscopy analysis (TEM) was carried out. Figure 3 presents, respectively, the TEM micrographs of the $Pr_{0.6}Bi_{0.4}Fe_xMn_{1-x}O_3$ powders heat treated at 900 °C for 4 h. Particles of few tens of nanometres to micrometre in size are observed.

Energy-dispersive analysis of X-ray (EDX)

Figure 4 shows the EDX spectra of all the sintered samples. It is clear from the EDX spectra that these samples are composed of Pr, Bi, Fe, and Mn elements. The presence of Cu is due to the grid support. The analysis of the amount of the different elements has been performed by EDX at room temperature. Regardless of the sample, the general composition is close to the expected $Pr_{0.6}Bi_{0.4}Fe_xMn_{1-x}O_3$ ($x = 0.1$, $x = 0.2$ and $x = 0.3$) formula. Local quantification highlights that for $x = 0.2$ and 0.3, the composition corresponds to the $Pr_{0.6}Bi_{0.4}Fe_xMn_{1-x}O_3$ formula, while for $x = 0.1$, local inhomogeneity is observed. Such results were confirmed by SEM measurement (see below). Of course, due to the presence of the $PrMn_2O_5$ minority phase, the exact composition of the perovskite structure is erroneous.

Scanning electron microscopy

The SEM images of the as-prepared and sintered samples are shown in Fig. 5a. SEM micrograph of the as-prepared sample reveals that regardless of the iron amount, the obtained $Pr_{0.6}Bi_{0.4}Fe_xMn_{1-x}O_3$ samples are porous and homogenous but with not a well-defined particle shape (see Fig. 5a for $x = 0.2$). On the other hand, the SEM micrographs (Fig. 5b) of the sintered samples evidence particles of well-defined shape. Interestingly, some modification of the particle shape is observed. While particles with a hexagonal shape are observed for $x = 0.1$, particles exhibiting cubic shape are observed for $x = 0.2$ and $x = 0.3$ (Fig. 6).

Magnetic properties

A systematic investigation of magnetization with temperature of all samples has been undertaken at very low applied magnetic field of 0.01 T (Fig. 7). The variation of the magnetization (M) versus temperature. (T) reveals that all

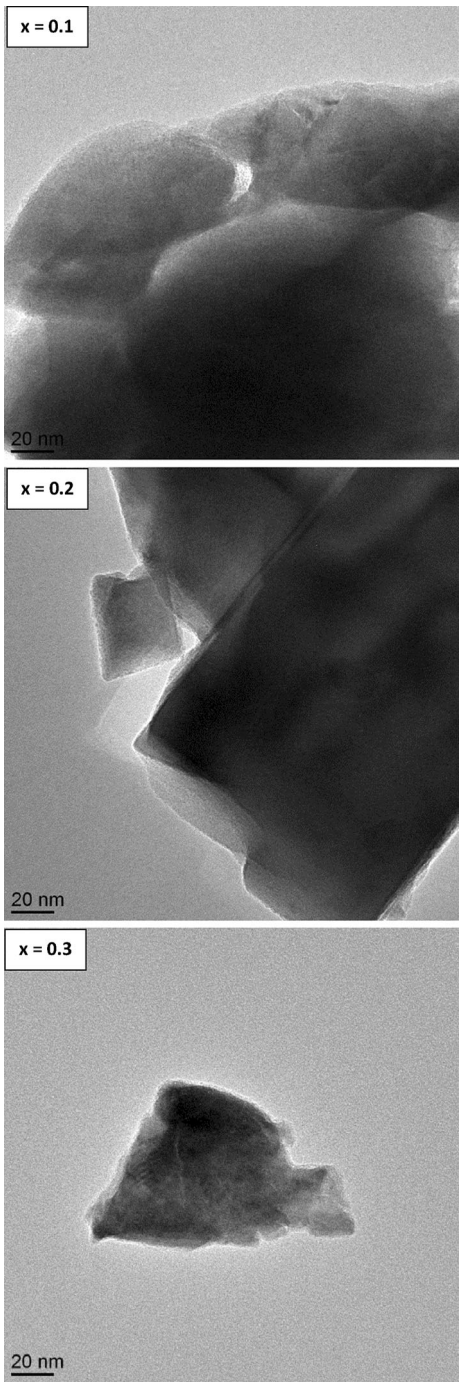

Fig. 3 Typical Transmission electron micrographs (TEM) of $Pr_{0.6}Bi_{0.4}Fe_xMn_{1-x}O_3$ compounds

samples exhibit a ferromagnetic–PM transition at Curie temperature. T_C—defined as the temperature at which dM/dT shows a maximum value. The obtained T_C values are found to be 40, 77, and 52 K for $x = 0.1$, 0.2, and 0.3, respectively. The evolution of T_C can be explained by the increased number of Fe^{3+}–O–Fe^{3+} interactions which indicates a weakening of ferromagnetism. This weakening

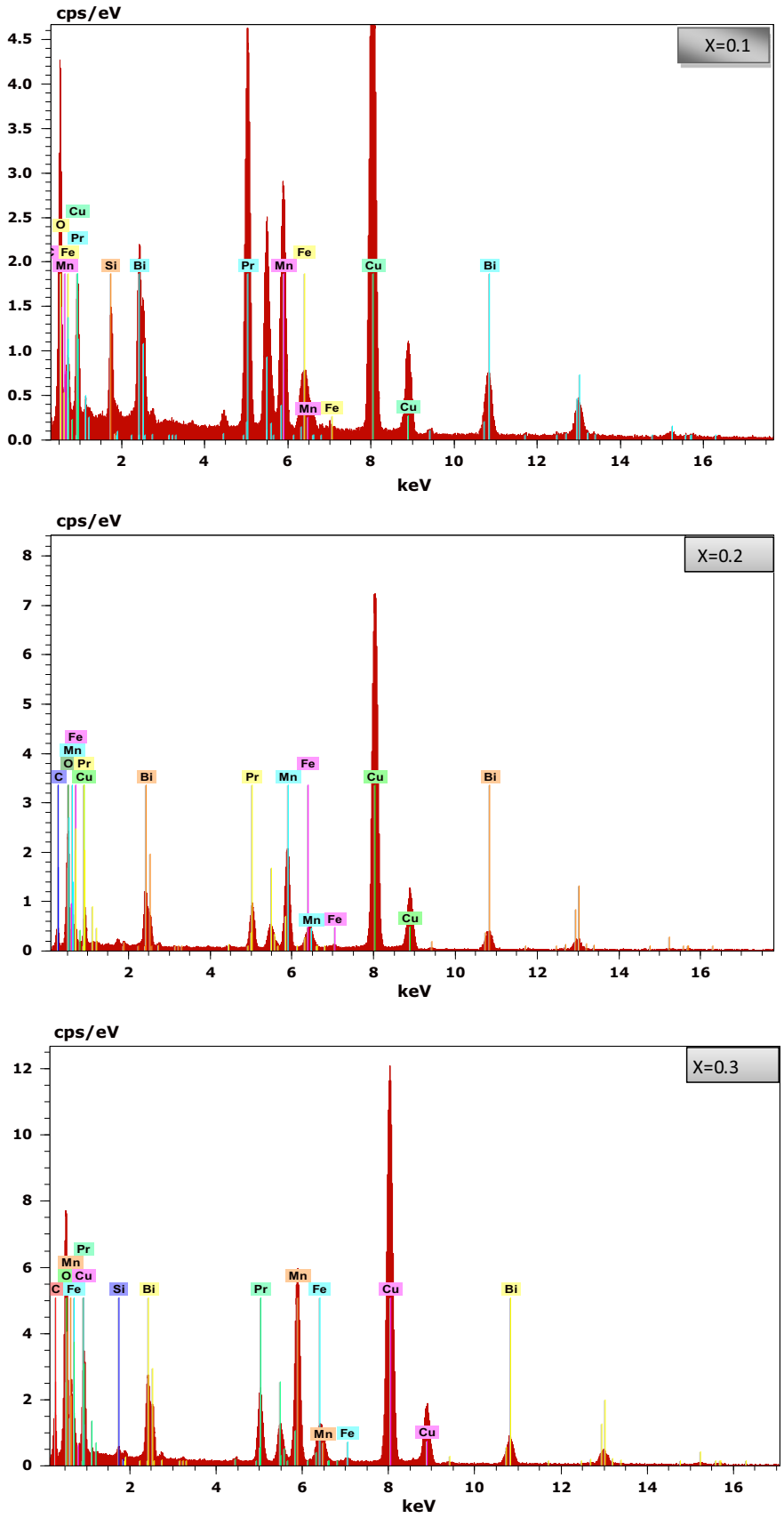

Fig. 4 EDAX analysis of $Pr_{0.6}Bi_{0.4}Fe_xMn_{1-x}O_3$ compounds

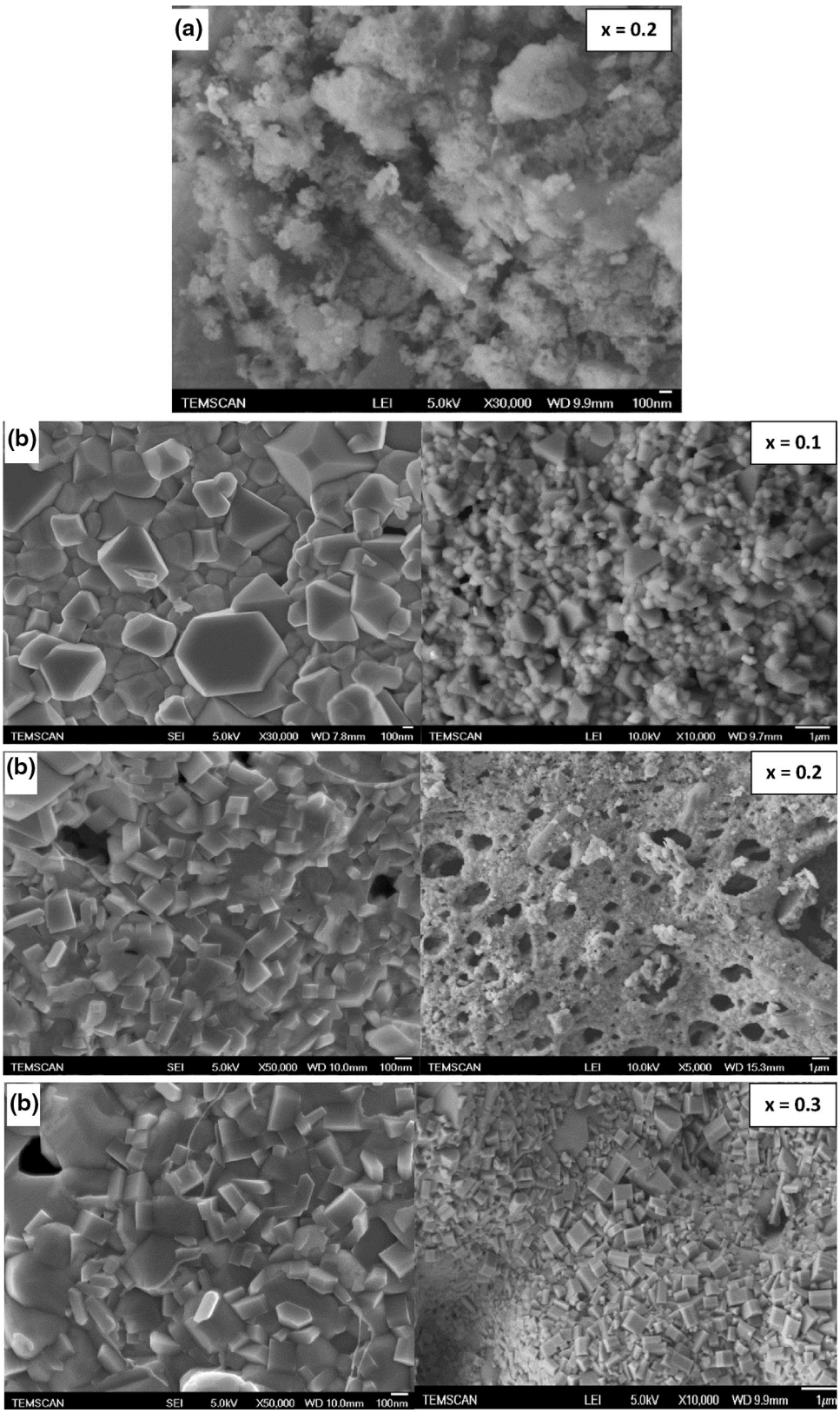

Fig. 5 Atomic distribution of $Pr_{0.6}Bi_{0.4}Fe_xMn_{1-x}O_3$ for ($x = 0.1$, $x = 0.2$ and $x = 0.3$)

can be explained by the competition between DE interaction Mn^{3+}–O–Mn^{4+} and superexchange antiferromagnetic interactions, typically Mn^{3+}–O–Mn^{3+} and Mn^{4+}–O–Mn^{4+}. The substitution of Mn by Fe giving rise to an antiferromagnetic coupling between Mn and Fe ions that favours the superexchange mechanism [23].

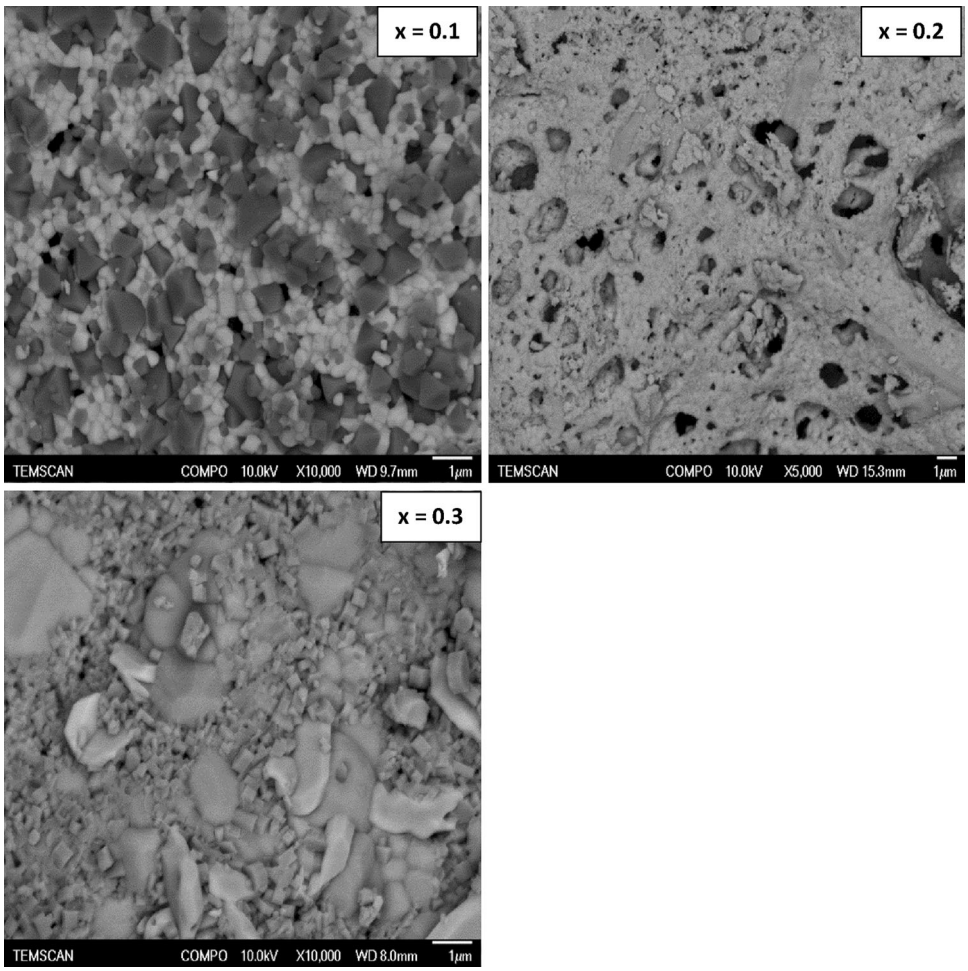

Fig. 6 Scanning transmission electron microscopy of $Pr_{0.6}Bi_{0.4}Fe_xMn_{1-x}O_3$ obtained at 900 °C/4 h

The PM–FM transition is also highlighted using a linear extrapolation to the zero magnetization of the χ^{-1}-(T) curves (Fig. 7). The Curie temperature of the $Pr_{0.6}Bi_{0.4}Fe_xMn_{1-x}O_3$ powders is similar to those obtained by Troyanchuk et al. and by Chen et al. [24, 25]. The magnetic properties of $PrMn_2O_5$ sample reveal that the oxide has antiferromagnetic transition at low temperature giving a Neel temperature (T_N) at 100 K.

In the PM region ($T \geq T_c$), the magnetization curve is well fitted by Curie–Weiss law (see Fig. 7 the inset). The temperature dependence of inverse magnetic susceptibility data in the 5–300 K temperature range follow a Curie–Weiss behavior above Tc. The relation between χ and temperature T should follow the Curie–Weiss law in the PM region:

$$\chi = \frac{C}{T - \theta p}, \tag{2}$$

where C and θp are the Curie constant and the Weiss temperature, respectively. C and θp were obtained by fitting the linear PM region of $\chi(T)$ curve (Table 1). The positive θp value indicates an FM interaction between the spins. The positive magnetic interaction in these compounds is due to the presence of Mn^{3+} and Fe^{3+} ions, which favor FM interaction. The obtained value is slightly higher than T_C. From these results, we can deduce that this difference depends on the substance and is related to the presence of short-range ordered slightly above the Curie temperature, which is related to the presence of magnetic inhomogeneity [26].

In order to gain a deeper understanding of the magnetic properties and to confirm the ferromagnetic behavior at low temperatures, the isothermal magnetic hysteresis loops, M (H), have been recorded. As seen in Fig. 8, the curve reveals a ferromagnetic property with a clear magnetic hysteresis at 2 K. From this figure, we see that magnetization decreases with the increasing Fe content. In fact, magnetization does not reach the saturation for $x = 0.2$ and $x = 0.3$. This confirms the presence of the AFM interactions, which are more important for higher Fe contents ($x = 0.2$ and $x = 0.3$) [27, 28].

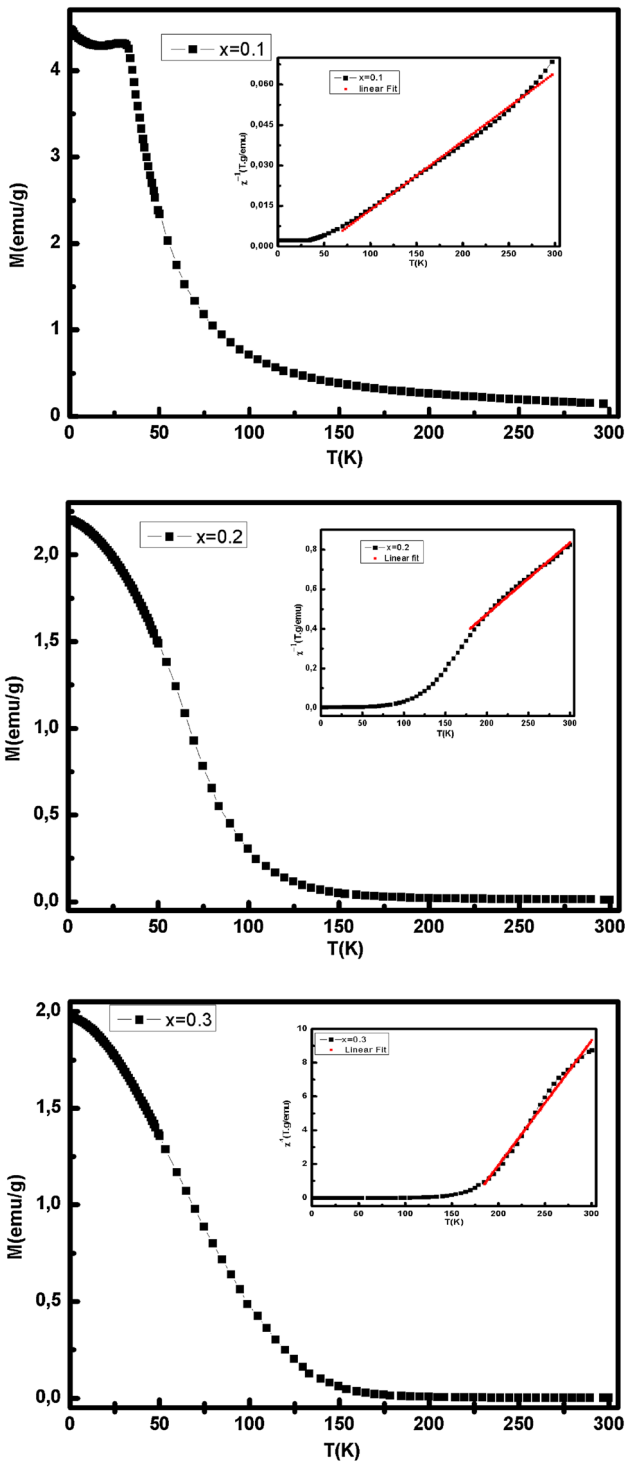

Fig. 7 Magnetization measurements as a function of temperature for $Pr_{0.6}Bi_{0.4}Fe_xMn_{1-x}O_3$. The *inset* Temperature dependent inverse magnetic susceptibility, χ^{-1} plot for $Pr_{0.6}Bi_{0.4}Fe_xMn_{1-x}O_3$ (**a** $x = 0.1$, **b** $x = 0.2$ and **c** $x = 0.3$) compounds

Magnetocaloric study

The MCE is an intrinsic property of magnetic materials. It is the response of the material to the application or removal of magnetic field, which is maximized when the material is near its magnetic ordering temperature (Curie temperature T_C). The evolution of magnetization (M) versus magnetic field (H) for the $x = 0.1$ and 0.3 composition, obtained at different temperatures (T), is shown in Fig. 9. These curves reveal a strong variation of magnetization around the Curie temperature indicating a possible large magnetic entropy change associated with the ferromagnetic–PM transition temperature.

In order to check the nature of the magnetic transitions for the nanopowder, we have used the criterion given by Banerjee [29]. This criterion consists in inspecting the slope of isotherm plots of M^2 versus H/M. From a thermodynamic point of view, it can be concluded that if all the curves have a positive slope, the magnetic transition is of the second-order type. On the other hand, if some of the curves show a negative slope at some point, the transition is of the first-order type. A more standard type of Arrott plots is observed. The plots exhibit a linear behavior, and the positive and negative slopes are clearly noted in the complete M^2 range. So, following Banerjee's criterion, we can conclude that the ferromagnetic-to-PM (FM–PM) phase transition in the samples is obviously of the second-order type for $x = 0.1$ and first-order type for $x = 0.3$ as shown in Fig. 9 (the inset).

The MCE of the materials can be derived from the Maxwell's thermodynamic relationship:

Table 1 Physical parameters of $Pr_{0.6}Bi_{0.4}Fe_xMn_{1-x}O_3$ ($0.1 \leq x \leq 0.3$) compounds

	θp (K)	T_C (K)	C (emu K/g T)
0.1	69.36	40	0.01441
0.2	72.14	77	0.01386
0.3	150	52	0.13156

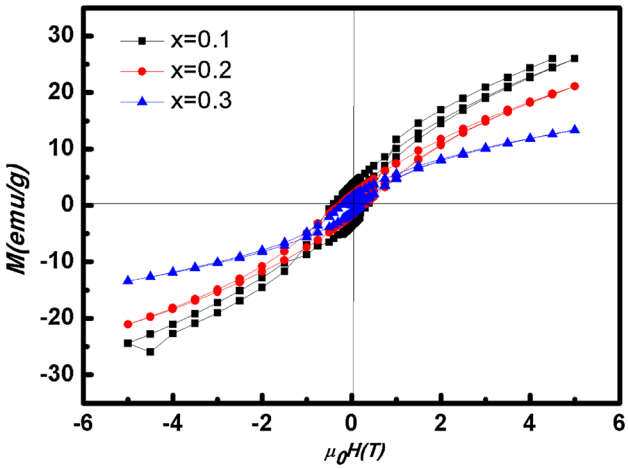

Fig. 8 Variation of magnetization as a function of applied magnetic field measured at 2 and 300 K for $Pr_{0.6}Bi_{0.4}Fe_xMn_{1-x}O_3$ compounds

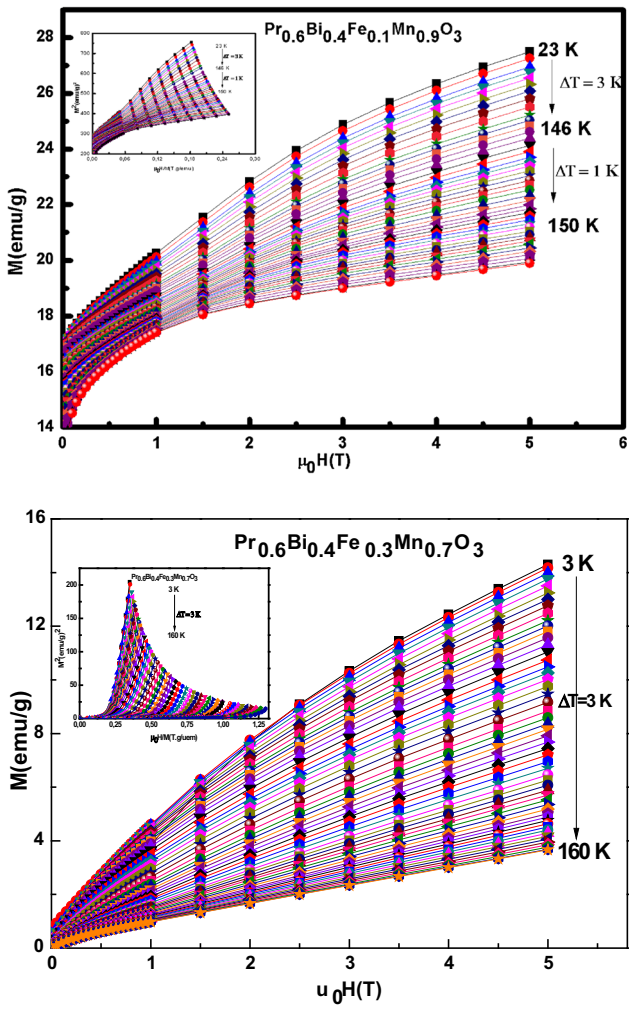

Fig. 9 Isothermal magnetization M (H) for $Pr_{0.6}Bi_{0.4}Mn_{0.9}Fe_{0.1}O_3$ and $Pr_{0.6}Bi_{0.4}Mn_{0.7}Fe_{0.3}O_3$.samples at several temperatures. The *inset* depicts *Arrot curves* M^2 versus μ_0H/M

$$\left(\frac{\partial H}{\partial T}\right)_{\mathrm{H}} = \left(\frac{\partial S}{\partial H}\right)_{\mathrm{T}}, \tag{3}$$

where S, M, and H are the magnetic entropy, the magnetization, and the applied magnetic field, respectively. The magnetic entropy change can be derived from Eq. (3) by integrating over the magnetic intensity H:

$$\Delta S_{\mathrm{M}}(H, T) = \int_0^H \frac{\partial M}{\partial T}\mathrm{d}H. \tag{4}$$

The values of the magnetic entropy changes (ΔS_{M}) upon application of magnetic fields from the isothermal M–H curve can be numerically calculated using Eq. (4):

$$\Delta S_{\mathrm{M}}\left(\frac{T_1+T_2}{2}\right) = \frac{1}{T_1+T_2} \times \left[\int_0^{H\max} M(T_2,H)dH - \int_0^{H\max} M(T_1,H)\mathrm{d}H\right] \tag{5}$$

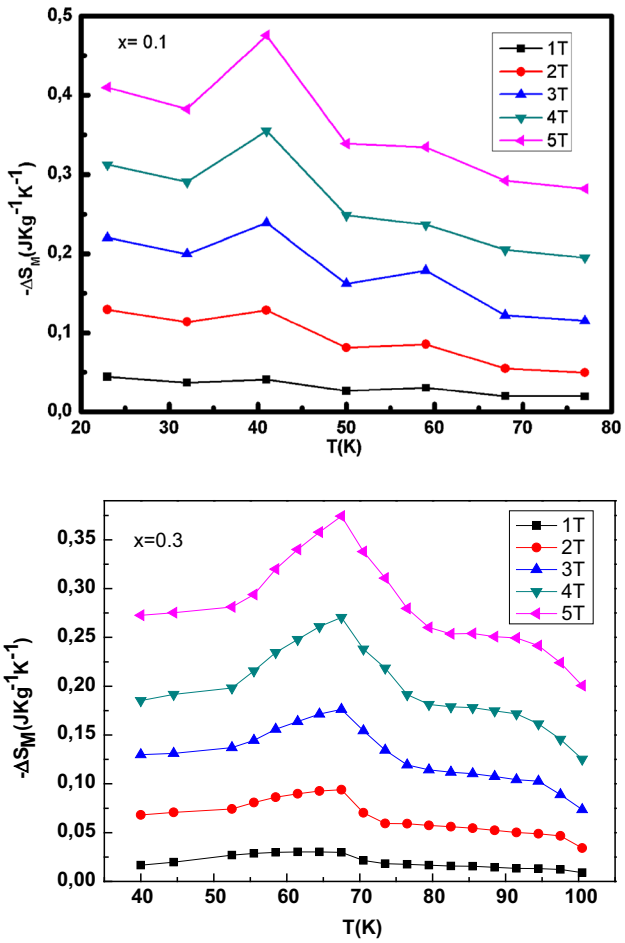

Fig. 10 Magnetic entropy change versus temperature for $Pr_{0.6}Bi_{0.4}Mn_{0.9}Fe_{0.1}O_3$ and $Pr_{0.6}Bi_{0.4}Mn_{0.7}Fe_{0.3}O_3$ samples at several applied magnetic field changes

Figure 10 shows the temperature dependence of $-\Delta S_{\mathrm{M}}$ (T, ($\Delta\mu_0 H$) for $x = 0.1$ and $x = 0.2$ for different applied magnetic fields. We can note that the magnetic entropy change depends on the magnetic applied field.

As expected, the overall value of entropy change is found to increase with the increasing field. Another notable feature is that increasing field shifts the magnetic transition temperature to higher temperatures. The maximum values of magnetic entropy change, ΔS_{M} are 0.47 and 0.37 J/kg/K for $x = 0.1$ and $x = 0.2$, respectively. But this field is not enough to saturate the sample. Compared with Gd 2.8 J/kg/K at 1 T field [30], $\Delta S_{\max}$ value is smaller for the present materials. However, these materials can be easily synthesized with good chemical stability. Another interesting feature in the MCE plot is that it is asymmetric, especially under high field. Similar behavior is observed in Si-substituted Lanthanum calcium manganite [31]. It is difficult to determine their RCP because of the non-uniform distribution of the ΔS_{M} curves. The non-uniform distribution of ΔS_{M} in nanocrystalline manganites is due to the enhanced grain

boundary effects and the spread of the ferromagnetic transition temperature in different magnetic clusters caused by the inhomogeneity of the structure and stoichiometry [31].

Conclusion

Morphologic, structural, magnetic, and magnetocaloric properties of $Pr_{0.6}Bi_{0.4}Fe_xMn_{1-x}O_3$ compounds have been investigated. X-ray diffraction showed that all samples crystallize in the orthorhombic system with *Pnma* space group. The FTIR spectra revealed the presence of the stretching and bending modes regardless of the samples. A PM–ferromagnetic transition of the second- and first-order type is observed for our materials. The magnetization versus magnetic field shows a small coercive field and an unsaturated magnetization which indicates that all samples are soft magnetic in nature at room temperature. From the magnetocaloric result, we demonstrate that the $Pr_{0.6}Bi_{0.4}Fe_{0.1}Mn_{0.9}O_3$ and $Pr_{0.6}Bi_{0.4}Fe_{0.3}Mn_{0.7}O_3$ samples present a magnetic entropy change ($-\Delta S_M$) being 0.47and 0.37 J/kg/K under an applied magnetic field change of 5 T. We can deduce that the presence of supplementary phases has no effect on the properties of manganites.

Acknowledgments This study has been supported by the Tunisian Ministry of Scientific Research and Technology. This research was also supported by the Centre National de la Recherche Scientifique, CNRS. Laure Vendier is acknowledged for PXRD measurements. The authors are grateful to the "Service Commun de Microscopie Electronique de L'Université Paul Sabatier" (TEMSCAN).

References

1. Gschneidner, K.A., Pecharsky, V.K.: Magnetocaloric materials. Annu. Rev. Mater. Sci. **30**, 387–429 (2000)
2. Pecharsky, V.K., Gschneidner, K.A.: Giant magnetocaloric effect in $Gd_5(Si_2Ge_2)$. J. Phys. Rev. Lett. **78**, 4494–4497 (1997)
3. Khlifi, M., Bejar, M., El Sadek, O., Dhahri, E., Ahmed, M.A., Hlil, E.K.: Structural, magnetic and magnetocaloric properties of the lanthanum deficient in $La_{0.8}Ca_{0.2-x}MnO_3$ (x = 0–0.20) manganites oxides. J. Alloys Compd. **509**, 7410–7415 (2011)
4. Oumezzine, E., Hcini, S., Baazaoui, M., Hlil, E.K., Oumezzine, M.: Structural, magnetic and magnetocaloric properties of $Zn_{0.6-x}Ni_xCu_{0.4}Fe_2O_4$ ferrite nanoparticles prepared by Pechini sol-gel method. Powder Technol. **278**, 189–195 (2015)
5. Sbissi, K., Kahn, M.L., Ellouze, M., Hlil, E.K., Elhalouani, F.: The magnetic and magnetocaloric properties of Pr_{1-x} Bi $_x$ MnO_3 ($x = 0.2$ and 0.4) manganites. J. Supercond. Novel. Magn. **28**, 1433–1438 (2015)
6. Othmani, S., Blel, R., Bejar, M., Sajieddine, M., Dhahri, E., Hlil, E.K.: New complex magnetic materials for an application in Ericsson refrigerator. Solid State Commun. **149**, 969–972 (2009)
7. Mori, S., Chen, C.H., Cheong, S.W.: Paired and unpaired charge stripes in the ferromagnetic phase of $La_{0.5}Ca_{0.5}MnO_3$. Phys. Rev. Lett. **81**, 33972–33975 (1998)
8. Cui, H., Zayat, M., Levy, D.: Sol-gel synthesis of nanoscaled spinels using propylene oxide as a gelation agent. Sol–Gel Sci. Technol. **35**, 175–181 (2005)
9. Gash, A., Tillotson, E., Satcher, T.M., Poco, J.H., Hrubesh, J.F., Hrubesh, L.W., Simpson, R.L.: Use of epoxides in the sol-gel synthesis of porous iron (III) oxide monoliths from Fe(III) salts. Chem. Mater. **33**, 999–1007 (2009)
10. Brinker, C.J., Scherer, G.W.: Sol–Gel Science: The Physics and Chemistry of Sol–Gel Processing. Academic Press, New York (1990)
11. Gaudon, M., Laberty-Robert, C., Ansart, F., Stevens, P., Rousset, A.: Preparation and characterization of $La_{1-x}Sr_xMnO_{3+\delta}$ ($0 \leq x \leq 0.6$) powder by sol gel processing. Solid State Sci. **4**, 125–133 (2002)
12. Keshri, S.S., Joshi, L., Kumar, R.S.: Influence of BTO phase on structural, magnetic and electrical properties of LCMO. J. Alloys Compd. **485**, 501–506 (2009)
13. Kolat, S., Gencer, H., Gunes, M., Atalay, S.: Effect of B-doping on the structural, magneto transport and magneto caloric properties of $La_{0.67}Ca_{0.33}MnO_3$ compounds. Mater. Sci. Eng. B. **140**, 212–217 (2007)
14. Roy, S., Bandyopadhyay, S.: Sol-gel synthesis of colloidal silica using cyclohexane. J. Mater. Sci. Lett. **15**, 1872–1874 (1996)
15. Nakamoto, K.: Infrared and Raman Spectra of Inorganic and Coordination Compounds, 3rd edn. Wiley, NewYork (1978)
16. Feng, Q., Yanagisawa, K., Yamasaki, N.: Hydrothermal soft chemical process for synthesis of manganese oxides with tunnel structures. J. Porous Mater. **5**, 153–161 (1998)
17. Zouari, S., Ellouze, M., Hlil, E.K., Elhalouani, F., Sajieddine, M.: Structural, morphologic and magnetic properties of $Pr_{0.6}La_{0.1}Ca_{0.3}Mn_{1-x}Fe_xO_3$ ($0 \leq x \leq 0.3$) perovskite nanopowder. J. Solid State Commun. **180**, 16–23 (2014)
18. Nasri, A., Zouari, S., Ellouze, M., Rehspringer, J.L., Lehlooh, A.F., Elhalouani, F.: Structural and magnetic properties of $Pr_{0.6}Sr_{0.4}Mn_{1-x}Fe_xO_3$ ($0 \leq x \leq 0.3$) manganites oxide prepared by the ball milling method. J. Supercond. Novel. Magn. **10**, 10948–22282 (2013)
19. Borchert, Y., Sonstrom, P., Wilhelm, M., Borchert, H., Balumer, M.: Nanostructured praseodymium oxide: preparation, structure, and catalytic properties. J. Phys. Chem. **112**, 3054–3063 (2008)
20. Alonso, J., Casais, A., Martinez-Lope, M.T., Rasines, M.J.: High oxygen pressure preparation, structural refinement and thermal behaviour of RMn_2O_5 (R = La, Pr, Nd, Sm, Eu). J. Solid State Chem. **129**, 105–112 (1997)
21. Popova, G., Greenblatta, M., Mc Carroll, W.H.: Synthesis of $LnMn_2O_5$ (Ln = Nd, Pr) crystals using fused salt electrolysis. Mater. Res. Bull. **35**, 1661–1667 (2000)
22. Vasylechko, L.: Semiconductor Electronic Dept, L'viv Polytechnic National Univ. ICDD Grant-in-Aid, Ukraine (2002)
23. Warren, B.E.: X-ray Diffraction. Dover Pub. Inc., New York (1990)
24. Nadeem, M., Akhtar, M.J., Khan, A.Y.: Effects of low frequency near metal-insulator transition temperatures on polycrystalline $La_{0.65}Ca_{0.35}Mn_1K_yFe_yO_3$ (where yz 0.05–0.10) ceramic oxides. Solid State Commun. **134**, 431–436 (2005)
25. Troyanchuk, I.O., Mantytskaja, O.S., Szymczak, H., Shvedun, M.Y.: Magnetic phase transitions in the system $La_{1-x}Bi_xMnO_{3+\lambda}$. Low Temp. Phys. **28**, 569–574 (2002)
26. Tozri, A., Dhahri, E., Hlil, E.K.: Effects of vacancy and Na doping on the structural, magnetic and transport properties of

$La_{0.8}Pb_{0.1}(/Na)_{0.1}MnO_3$. J. Magn. Magn. Mater. **322**, 2516–2524 (2010)
27. Cherif, R., Hlil, E.K., Ellouze, M., Elhalouani, F., Obbade, S.: Magnetic and magnetocaloric properties of $La_{0.6}Pr_{0.1}Sr_{0.3}Mn_{1-x}Fe_xO_3$ ($0 \leq x \leq 0.3$) manganites. J. Solid State Chem. **215**, 271–276 (2014)
28. Issaoui, F., Tlili, M., Bejar, M., Dhahri, E., Hlil, E.K.: Structural and magnetic studies of Ca_{2-x} Sm_x MnO_3 Compounds ($x = 0$–0.4). J. Supercond. Novel. Magn. **25**, 1169–1175 (2012)
29. Banerjee, B.K.: On a generalised approach to first and second order magnetic transitions. Phys. Lett. **12**, 16–17 (1964)
30. Ritter, C., Ibarra, M.R., De Teresa, J.M., Algarabel, P.A., Marquina, C., Blasco, J., Garcia, J., Oseroff, S., Cheong, S.W.: Influence of oxygen content on the structural, magnetotransport, and magnetic properties of $LaMnO_{3+\delta}$. Phys. Rev. B. **56**, 8902–8911 (1997)
31. Li, L., Nishimura, K., Fujii, M., Mori, K.: Effect of Mn-site Si substitution on magnetic, transport properties and colossal magnetoresistance in $La_{2/3}Ca_{1/3}Mn_{1-x}Si_xO_3$ ($x = 0.05$–0.25) system. Solid State Commun. **144**, 10–14 (2007)